Electronic Supporting Information (ESI)

for

A novel symmetric pyrazine (pyz)-bridged uranyl dimer $[UO_2Cl_3(H_2O)(Pyz)_{0.5}]_2^{2-}$: Synthesis, structural and computational analysis

Nicole M. Byrne,[a] Mark H. Schofield,[a] and Christopher L. Cahill[a*]

[a]Department of Chemistry, The George Washington University, 800 22nd St. NW, Suite 4000, Washington, D.C., 20052

Table of Contents

Chart S1: Input structural search parameters and CSD results used to interrogate possible other pyrazine bridged complexes and bridged dimers of interest.

Structural Search Parameters	CSD Results (CSD Code)[1]
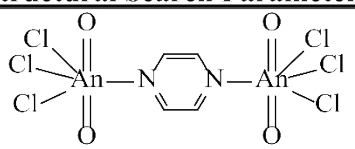	N/A
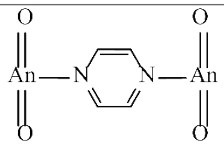	PUQJOB[2]
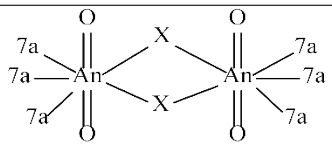	BZAPXU10[3] HOYXAU[4] HOYXAU01[4]
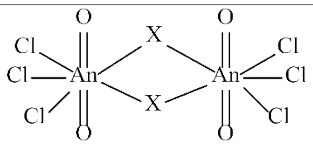	BZAPXU10[3]
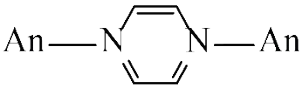	EYEREF[5] EYERIJ[5] IBADAT[6] PUQJOB[2] QORGIO[7] UYANUE[8]
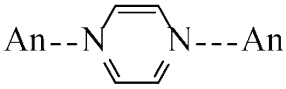	EYEREF[5] EYERIJ[5] IBADAT[6] JOJMEB[9] PUQJOB[2] QORGIO[7] SODCOE[10] SODCUK[10] UYANUE[8]
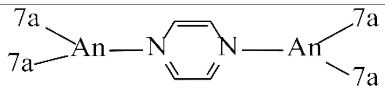	N/A
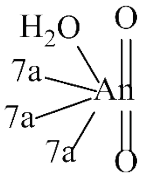	NATJUR[11] BEZLEX[12] CAWGAJ[13] CURCRO[14] DAPWUM[15] DUFTUW[16] NILBAL[17] NILBAL01[18] SIRJIO[19] TEAUFO10[20] XEVRAS[21] XEVRAS01[22] XIHSAL[22] XIHSEP[22] XIHSIT[22] ZAHSOT[23]

Table S1: Crystallography table for compound **1**.

	1
Chemical Formula	$(C_4H_5N_2)_2[UO_2Cl_3(H_2O)(C_4H_4N_2)_{0.5}]_2{\cdot}2H_2O$
Formula Weight (g/mol)	1067.1
Crystal System	Triclinic
Space Group	P-1
***a* (Å)**	7.3929(3)
***b* (Å)**	8.7830(5)
***c* (Å)**	12.2365(6)
α (°)	70.837(2)
β (°)	73.478(2)
γ (°)	69.922(3)
V (Å^3)	691.57(9)
Z	1
T (K)	100(2)
λ (Mo Kα)	0.71073
μ (mm^{-1})	12.319
R_{int}	0.0262
R_1	0.0106
wR2	0.0256

Table S2: Bond distances and angles for compound **1**, $(HPyz^{+})_2[UO_2Cl_3(H_2O)(Pyz)_{0.5}]_2 \cdot 2H_2O$.

Atom(1)-Atom(2)	Bond distance (Å)	Atom(1)-Atom(2)-Atom(3)	Bond angle (°)	Atom(1)-Atom(2)-Atom(3)	Bond Angle (°)
U(1)-O(2)	1.7640(15)	O(2)-U(1)-O(1)	175.82(7)	C(5)-C(6)-H(6)	118.9
U(1)-O(1)	1.7654(14)	O(2)-U(1)-O(5)	90.05(7)	N(4)-C(7)-C(8)	122.1(2)
U(1)-O(5)	2.4385(15)	O(1)-U(1)-O(5)	91.84(6)	N(4)-C(7)-H(7)	118.9
U(1)-N(1)	2.5979(19)	O(2)-U(1)-N(1)	85.91(7)	C(8)-C(7)-H(7)	118.9
U(1)-Cl(2)	2.6895(6)	O(1)-U(1)-N(1)	90.24(6)	N(3)-C(8)-C(7)	118.3(2)
U(1)-Cl(3)	2.7121(5)	O(5)-U(1)-N(1)	139.95(6)	N(3)-C(8)-H(8)	120.9
U(1)-Cl(1)	2.7543(5)	O(2)-U(1)-Cl(2)	91.55(6)	C(7)-C(8)-H(8)	120.9
O(5)-H(5A)	0.8699	O(1)-U(1)-Cl(2)	92.59(5)	H(7B)-O(7)-H(7A)	110(3)
O(5)-H(5B)	0.8699	O(5)-U(1)-Cl(2)	71.79(4)		
N(1)-C(2)	1.340(3)	N(1)-U(1)-Cl(2)	148.04(4)		
N(1)-C(1)	1.342(3)	O(2)-U(1)-Cl(3)	90.72(5)		
C(1)-C(2)#1	1.377(3)	O(1)-U(1)-Cl(3)	89.50(5)		
C(1)-H(1)	0.95	O(5)-U(1)-Cl(3)	150.01(4)		
C(2)-H(2)	0.95	N(1)-U(1)-Cl(3)	69.97(4)		
N(3)-C(8)	1.328(3)	Cl(2)-U(1)-Cl(3)	78.219(16)		
N(3)-C(5)	1.336(3)	O(2)-U(1)-Cl(1)	90.83(5)		
N(3)-H(3)	0.8801	O(1)-U(1)-Cl(1)	86.31(5)		
N(4)-C(7)	1.329(3)	O(5)-U(1)-Cl(1)	70.30(4)		
N(4)-C(6)	1.337(3)	N(1)-U(1)-Cl(1)	69.94(4)		
C(5)-C(6)	1.373(3)	Cl(2)-U(1)-Cl(1)	142.010(17)		
C(5)-H(5)	0.95	Cl(3)-U(1)-Cl(1)	139.657(17)		
C(6)-H(6)	0.95	U(1)-O(5)-H(5A)	127.1		
C(7)-C(8)	1.378(3)	U(1)-O(5)-H(5B)	127.9		
C(7)-H(7)	0.95	H(5A)-O(5)-H(5B)	104.5		
C(8)-H(8)	0.95	C(2)-N(1)-C(1)	116.4(2)		
O(7)-H(7B)	0.804(17)	C(2)-N(1)-U(1)	120.79(14)		
O(7)-H(7A)	0.791(17)	C(1)-N(1)-U(1)	122.68(15)		
		N(1)-C(1)-C(2)#1	121.7(2)		
		N(1)-C(1)-H(1)	119.1		
		C(2)#1-C(1)-H(1)	119.1		
		N(1)-C(2)-C(1)#1	121.9(2)		
		N(1)-C(2)-H(2)	119.1		
		C(1)#1-C(2)-H(2)	119.1		
		C(8)-N(3)-C(5)	121.7(2)		
		C(8)-N(3)-H(3)	119.1		
		C(5)-N(3)-H(3)	119.2		
		C(7)-N(4)-C(6)	117.7(2)		
		N(3)-C(5)-C(6)	118.1(2)		
		N(3)-C(5)-H(5)	120.9		
		C(6)-C(5)-H(5)	120.9		
		N(4)-C(6)-C(5)	122.1(2)		
		N(4)-C(6)-H(6)	118.9		

Figure S1: ORTEP drawing of compound **1**, $(HPyz^{+})_2[UO_2Cl_3(H_2O)(Pyz)_{0.5}]_2 \cdot 2H_2O$.

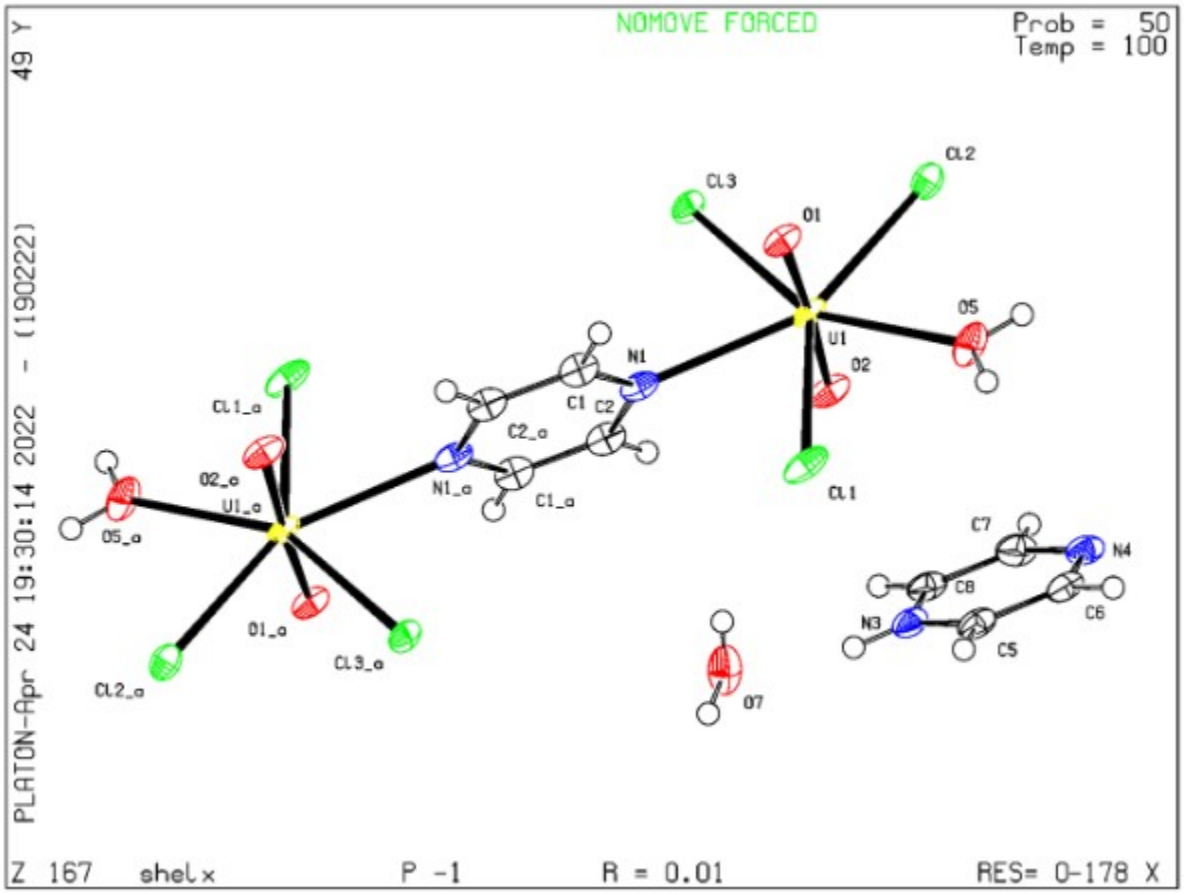

Figure S2: Room temperature UV-Visible-DRS spectrum of compound 1, $(HPyz^{+})_2[UO_2Cl_3(H_2O)(Pyz)_{0.5}]_2 \cdot 2H_2O$.

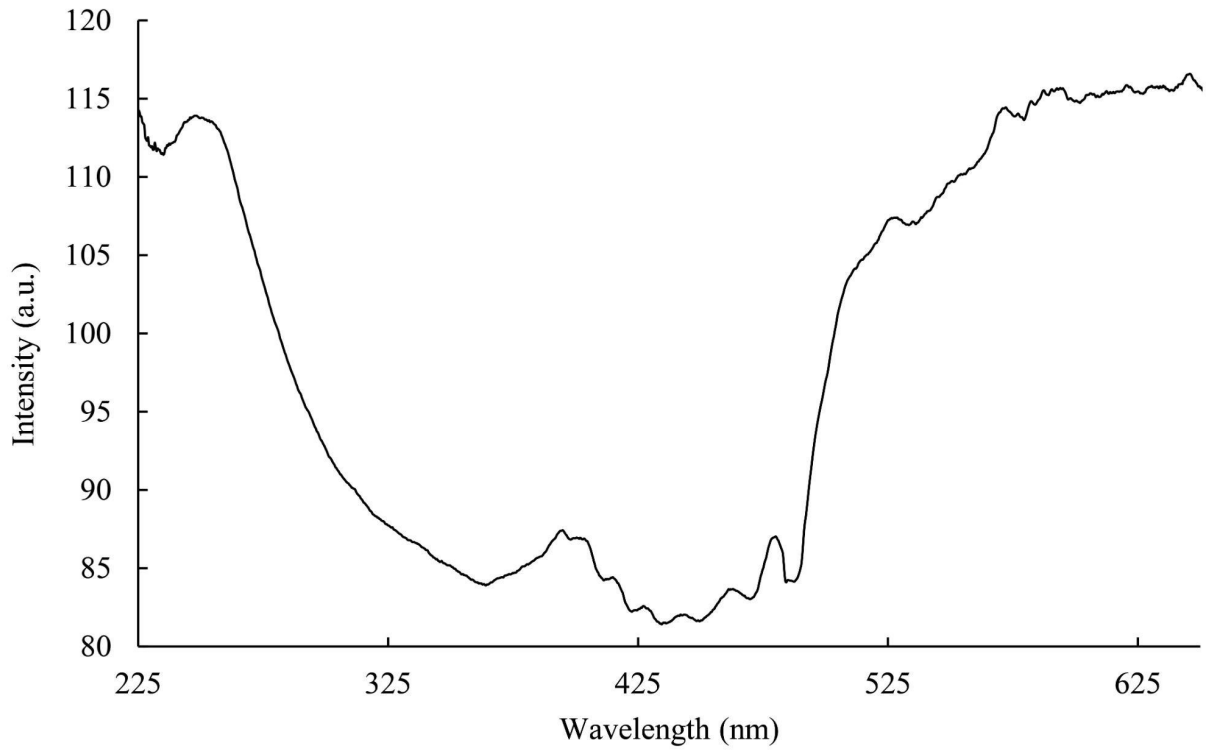

Figure S3: Room temperature Raman spectrum of compound 1, $(HPyz^{+})_2[UO_2Cl_3(H_2O)(Pyz)_{0.5}]_2 \cdot 2H_2O$, using a 532 nm excitation line.

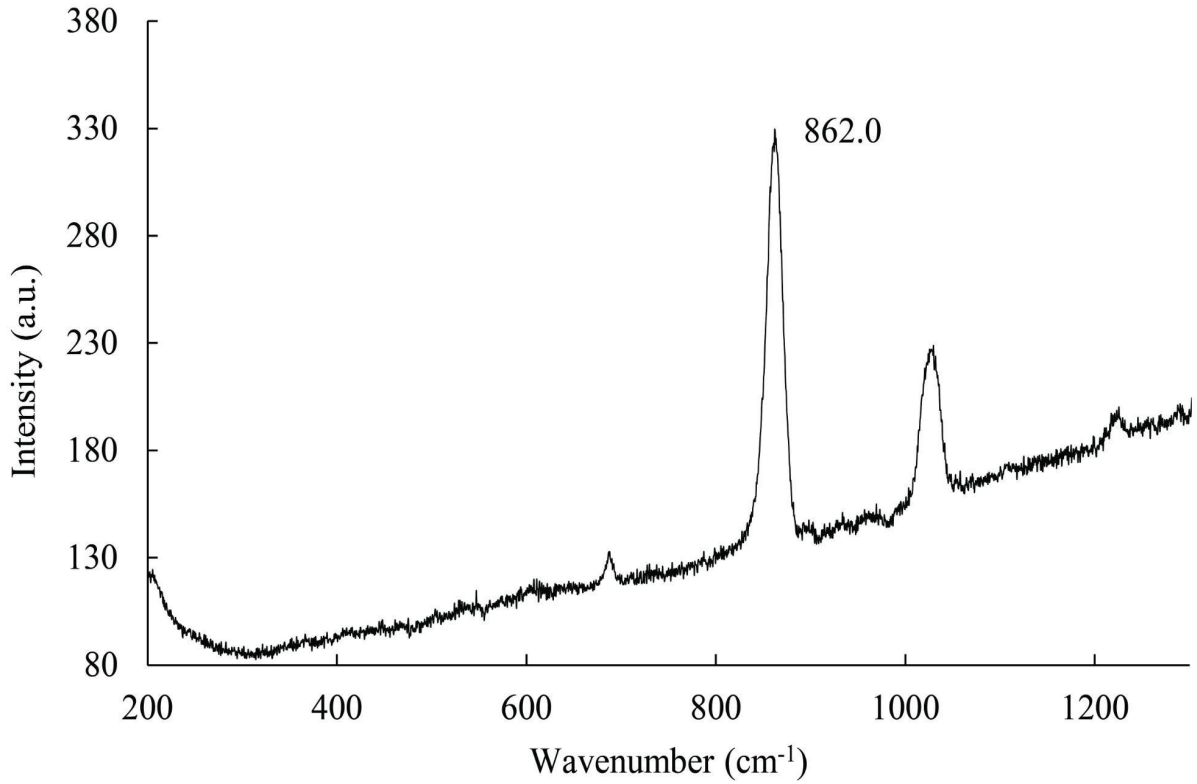

Figure S4: Model of the isolated $[UO_2Cl_3(H_2O)(Pyz)_{0.5}]_2^{2-}$ anion, with relevant atoms labeled, which was utilized for all DFT and QTAIM calculations.

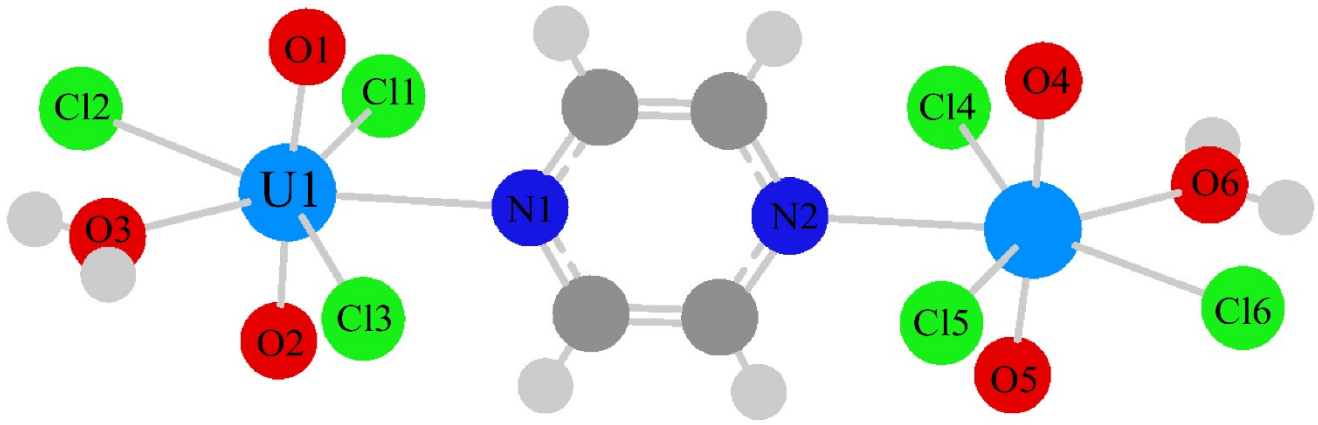

Figure S5: Side-by-side comparison of the unoptimized and optimized $[UO_2Cl_3(H_2O)(Pyz)_{0.5}]_2^{2-}$ dimer from the top, in order to show the rotation of the equatorial bridging pyrazine and water molecules.

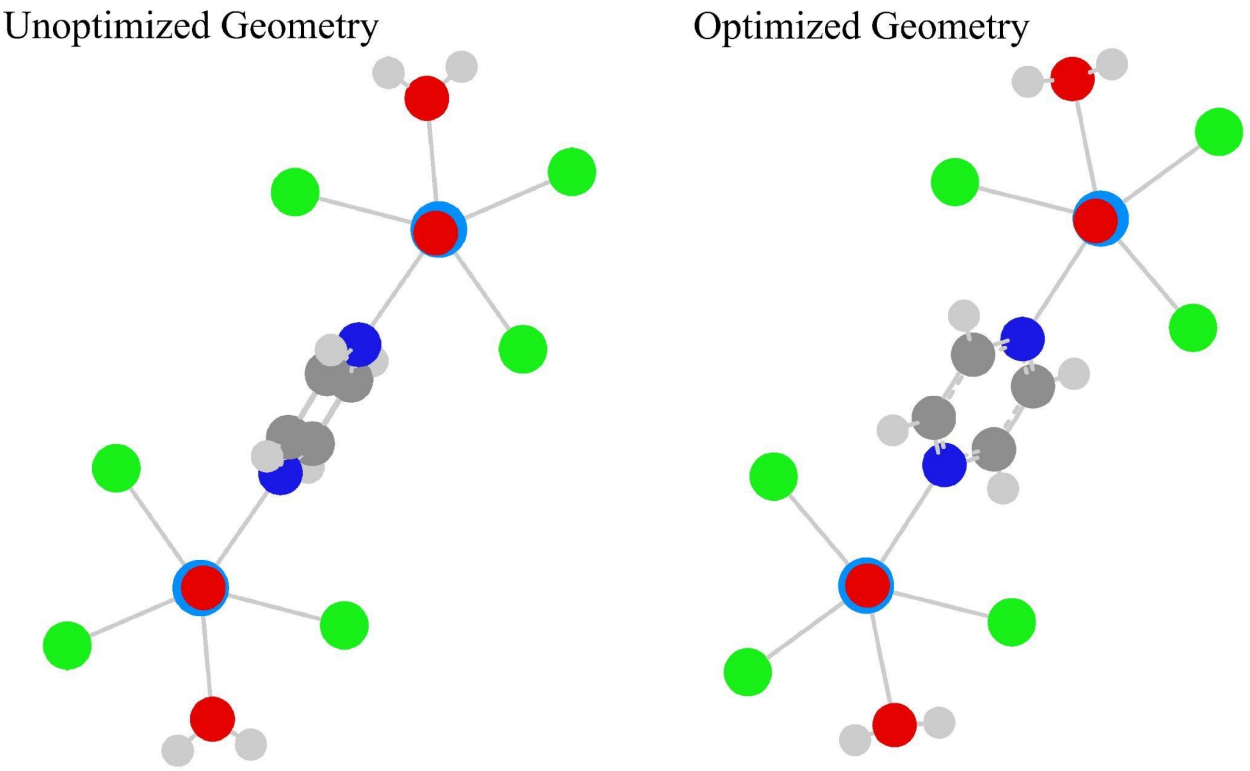

Figure S6: Model of the isolated $[UO_2Cl_4]^{2-}$ dianion, with relevant atoms labeled, which was used for all DFT and QTAIM calculations.

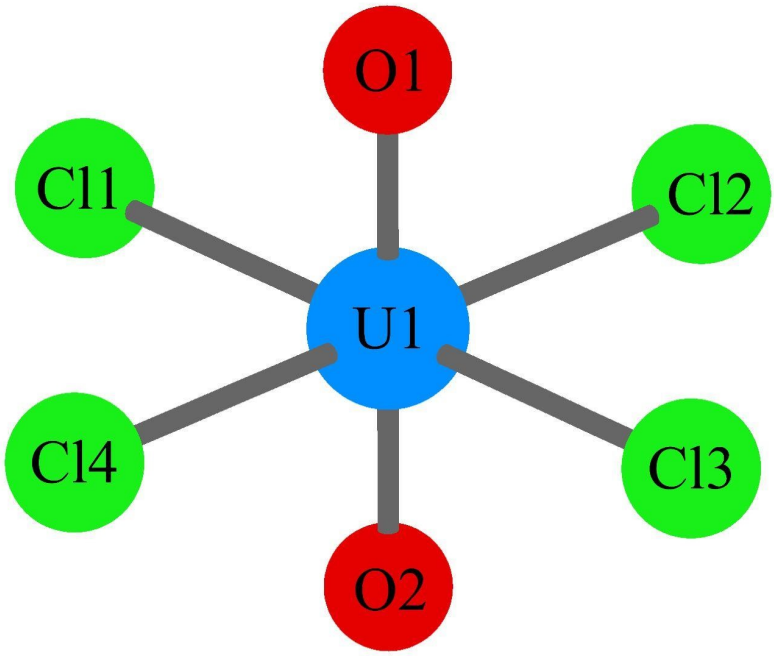

Figure S6: Isodensity representation of the (Left) equatorial chloride p orbitals that comprise the HOMO of the $[UO_2Cl_4]^{2-}$ dianion and (Right) pure 5f orbitals, which serve as the LUMO of $[UO_2Cl_4]^{2-}$.

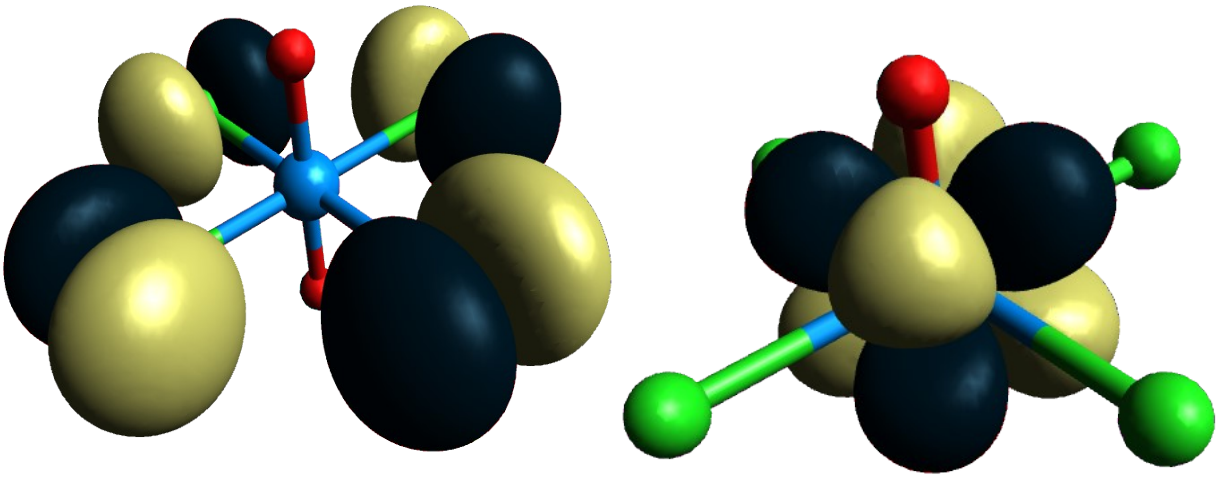

Table S3: Calculated Raman and IR frequencies and atomic displacements for the symmetric and asymmetric stretches of the $[UO_2Cl_3(H_2O)(Pyz)_{0.5}]_2^{2-}$ dianion.

	51			**52**			**53**			**54**		
	AU			AG			AG			AG		
Frequencies	870.311			870.3182			918.0632			948.031		
Red. masses	15.8616			14.5217			1.2732			16.3255		
Frc consts	7.0786			6.4807			0.6323			8.6449		
IR Inten	4.6401			0			0			0		
Raman Activ	0			146.4454			4.4593			0.569		
Depolar (P)	0			0.0052			0.1817			0.5318		
Depolar (U)	0			0.0103			0.3076			0.6943		
Atom /AN	X	Y	Z	X	Y	Z	X	Y	Z	X	Y	Z
1 92	0.00	0.00	0.00	0.00	0.00	0.00	0.00	0.00	0.00	-0.04	-0.05	0.03
2 17	0.01	-0.01	0.00	0.01	-0.01	0.00	0.00	0.00	0.00	0.00	0.00	0.00
3 17	-0.01	0.00	-0.01	-0.01	0.00	-0.01	0.00	0.00	0.00	0.00	0.00	0.00
4 17	0.00	0.01	0.01	0.00	0.01	0.01	0.00	0.00	0.00	0.00	0.00	0.00
5 8	0.30	0.35	-0.21	0.29	0.33	-0.20	0.01	0.01	-0.01	0.27	0.31	-0.19
6 8	-0.27	-0.35	0.21	-0.25	-0.33	0.20	-0.01	-0.01	0.00	0.26	0.35	-0.21
7 8	0.00	-0.01	-0.01	-0.01	-0.01	-0.01	0.00	0.00	0.00	0.00	0.00	0.00
8 1	0.02	0.02	0.03	0.02	0.02	0.02	0.00	0.00	0.00	-0.01	-0.03	-0.06
9 1	0.00	0.02	-0.01	0.00	0.02	0.00	0.00	0.00	0.00	-0.02	-0.02	-0.06
10 7	0.00	0.00	0.00	0.00	0.00	0.00	0.00	0.00	0.00	0.00	0.01	0.01
11 6	0.01	-0.01	0.00	0.01	-0.02	-0.02	0.00	0.07	0.02	0.01	-0.04	0.00
12 1	0.01	0.05	0.01	-0.01	0.15	0.02	0.00	-0.48	-0.13	-0.02	0.16	0.05
13 6	0.00	0.01	0.01	-0.02	0.02	0.01	0.00	-0.07	-0.02	-0.01	-0.03	-0.02
14 1	0.00	-0.03	0.00	-0.02	-0.15	-0.05	-0.01	0.48	0.12	-0.01	0.10	0.05
15 7	0.00	0.00	0.00	0.00	0.00	0.00	0.00	0.00	0.00	0.00	-0.01	-0.01
16 6	0.01	-0.01	0.00	-0.01	0.02	0.02	0.00	-0.07	-0.02	-0.01	0.04	0.00
17 1	0.01	0.05	0.01	0.01	-0.15	-0.02	0.00	0.48	0.13	0.02	-0.16	-0.05
18 6	0.00	0.01	0.01	0.02	-0.02	-0.01	0.00	0.07	0.02	0.01	0.03	0.02
19 1	0.00	-0.03	0.00	0.02	0.15	0.05	0.01	-0.48	-0.12	0.01	-0.10	-0.05
20 92	0.00	0.00	0.00	0.00	0.00	0.00	0.00	0.00	0.00	0.04	0.05	-0.03
21 17	0.01	-0.01	0.00	-0.01	0.01	0.00	0.00	0.00	0.00	0.00	0.00	0.00
22 17	-0.01	0.00	-0.01	0.01	0.00	0.01	0.00	0.00	0.00	0.00	0.00	0.00
23 17	0.00	0.01	0.01	0.00	-0.01	-0.01	0.00	0.00	0.00	0.00	0.00	0.00
24 8	0.30	0.35	-0.21	-0.29	-0.33	0.20	-0.01	-0.01	0.01	-0.27	-0.31	0.19
25 8	-0.27	-0.35	0.21	0.25	0.33	-0.20	0.01	0.01	0.00	-0.26	-0.35	0.21
26 8	0.00	-0.01	-0.01	0.01	0.01	0.01	0.00	0.00	0.00	0.00	0.00	0.00
27 1	0.02	0.02	0.03	-0.02	-0.02	-0.02	0.00	0.00	0.00	0.01	0.03	0.06
28 1	0.00	0.02	-0.01	0.00	-0.02	0.00	0.00	0.00	0.00	0.02	0.02	0.06

Figure S7: Calculated Raman spectra rendered from B3LYP outputs. An inset is provided to highlight the U=O ν_1 region from 790 to 900 cm^{-1}.

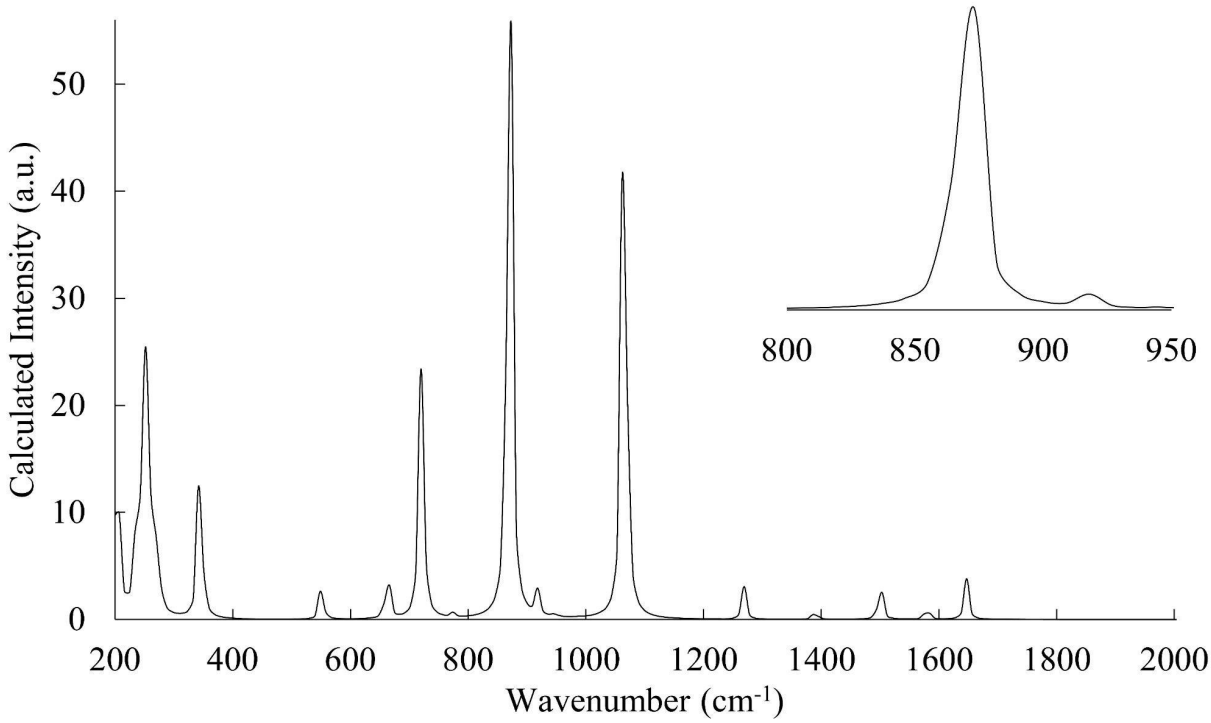

Table S4: Calculated Raman and IR frequencies and atomic displacements for $[UO_2Cl_4]^{2-}$ in the uranyl symmetric stretch region (ν = 750-900 cm^{-1}).

	14			**15**		
	AG			AU		
Frequencies	862.6125			942.2844		
Red. masses	16.0154			18.1577		
Frc consts	7.0213			9.4989		
IR Inten	0.0000			336.0006		
Raman Activ	73.0829			0.0000		
Depolar (P)	0.0005			0.0000		
Depolar (U)	0.0011			0.0000		
Atom/ AN	X	Y	Z	X	Y	Z
1 92	0.00	0.00	0.00	0.02	0.04	-0.09
2 17	0.01	-0.01	0.00	0.00	0.00	0.01
3 17	-0.01	-0.01	-0.01	0.00	0.00	0.01
4 8	-0.18	-0.25	0.64	-0.17	-0.25	0.63
5 17	-0.01	0.01	0.00	0.00	0.00	0.01
6 17	0.01	0.01	0.01	0.00	0.00	0.01
7 8	0.18	0.25	-0.64	-0.17	-0.25	0.63

Table S5: Method validation across B3LYP, BLYP, CAM-B3LYP, BP86, PBE1PBE and TPSSH functionals for the $[UO_2Cl_3(H_2O)(Pyz)_{0.5}]_2^{2-}$ computational model, using Wiberg bond indices as a reference metric. Although slight deviations in index values occur across functionals, we observe the same trends in bonding, supporting the validity of the model and the lack of potential functional bias, further supported by low standard deviations.

	B3LYP	BLYP	CAM-B3LYP	BP86	PBE1PBE	TPSSH	Std. Dev. (%)
U=O1	2.0695	2.0923	2.0653	2.1065	2.0774	2.0820	-
U=O2	2.0645	2.0873	2.0602	2.1015	2.0724	2.0869	-
U=O Average	2.0670	2.0898	2.0628	2.1040	2.0749	2.0845	1.54
U-Cl1	0.7663	0.8201	0.7359	0.8265	0.7603	0.7874	-
U-Cl2	0.8575	0.9195	0.8225	0.9256	0.8490	0.8807	-
U-Cl3	0.8749	0.9484	0.8329	0.9544	0.8643	0.9024	-
Average U-Cl	0.8329	0.8960	0.7971	0.9022	0.8245	0.8568	4.15
U-N1	0.3247	0.3427	0.3152	0.3467	0.3230	0.3329	1.22
U-OH_2	0.3157	0.3271	0.3136	0.3330	0.3164	0.3231	0.76

Table S5: Method validation across B3LYP, BLYP, CAM-B3LYP, BP86, PBE1PB3 and TPSSH functionals for the $[UO_2Cl_4]^{2-}$ computational model, using Wiberg bond indices as a reference metric. Although slight deviations in index values occur across functionals, we observe the same trends in bonding, supporting the validity of the model and the lack of potential functional bias, further supported by low standard deviations.

	B3LYP	BLYP	CAM-B3LYP	BP86	PBE1PBE	TPSSH	Std. Dev. (%)
U=O1	2.0540	2.0771	2.0495	2.0911	2.0621	2.0719	-
U=O2	2.0540	2.0771	2.0495	2.0910	2.0621	2.0719	-
U=O Average	2.0540	2.0771	2.0495	2.0911	2.0621	2.0719	1.55
U-Cl1	0.8235	0.8755	0.7925	0.8815	0.816	0.8418	-
U-Cl2	0.8424	0.8945	0.8101	0.9007	0.8349	0.8609	-
U-Cl3	0.8237	0.8757	0.7923	0.8817	0.8162	0.8420	-
U-Cl4	0.8415	0.8936	0.8110	0.8998	0.8340	0.8600	-
U-Cl Average	0.8328	0.8848	0.8015	0.8909	0.8253	0.8512	3.50

References

1. Groom CR, Bruno IJ, Lightfoot MP, Ward SC. The Cambridge Structural Database. Acta Cryst B. 2016 Apr 1;72(2):171–9. CSD version: 5.43, update 1: [cited 2022 June 16].

2. Thuéry P, Masci B. Uranyl Ion Complexation by Cucurbiturils in the Presence of Perrhenic, Phosphoric, or Polycarboxylic Acids. Novel Mixed-Ligand Uranyl−Organic Frameworks. Crystal Growth & Design. 2010 Feb 3;10(2):716–25.

3. Haegele R, Boeyens JCA. Crystal structure of benzyltrimethylammonium μ2-peroxo-bis[trichlorodioxouranate(VI)], a binuclear uranium complex containing dioxygen in a μ2-peroxo-linkage. J Chem Soc, Dalton Trans. 1977 Jan 1;(7):648–50.

4. Walker SM, Halasyamani PS, Allen S, O'Hare D. From Molecules to Frameworks: Variable Dimensionality in the UO2(CH3COO)2·2H2O/HF(aq)/Piperazine System. Syntheses, Structures, and Characterization of Zero-Dimensional (C4N2H12)UO2F4·3H2O, One-Dimensional (C4N2H12)2U2F12·H2O, Two-Dimensional (C4N2H12)2(U2O4F5)4·11H2O, and Three-Dimensional (C4N2H12)U2O4F6. J Am Chem Soc. 1999 Nov 1;121(45):10513–21.

5. Mehdoui T, Berthet JC, Thuéry P, Ephritikhine M. Clear-Cut Lanthanide(III)/Actinide(III) Differentiation in Coordination of Pyrazine to Tris(cyclopentadienyl) Complexes of Cerium and Uranium, Involving Reversible UIII → UIV Oxidation. European Journal of Inorganic Chemistry. 2004;2004(10):1996–2000.

6. Severance, R. C., Smith, M. D., zur Loye, H. C. *CSD Communication*, 2016. CCDC: 827123.

7. Evans WJ, Takase MK, Ziller JW, DiPasquale AG, Rheingold AL. Reductive Reactivity of the Tetravalent Uranium Complex [(η5-C5Me5)(η8-C8H8)U]2(μ-η3:η3-C8H8). Organometallics. 2009 Jan 12;28(1):236–43.

8. Monreal MJ, Khan SI, Kiplinger JL, Diaconescu PL. Molecular quadrangle formation from a diuranium μ-η6,η6-toluene complex. Chem Commun. 2011 Aug 2;47(32):9119–21.

9. Frisch M, Cahill CL. Thorium(IV) Coordination Polymers in the Pyridine and Pyrazinedicarboxylic Acid Systems. Crystal Growth & Design. 2008 Aug 1;8(8):2921–8.

10. Masci B, Thuéry P. Pyrazinetetracarboxylic Acid as an Assembler Ligand in Uranyl−Organic Frameworks. Crystal Growth & Design. 2008 May 1;8(5):1689–96.

11. Hu KQ, Zeng LW, Kong XH, Huang ZW, Yu JP, Mei L, et al. Viologen-Based Uranyl Coordination Polymers: Anion-Induced Structural Diversity and the Potential as a Fluorescent Probe. European Journal of Inorganic Chemistry. 2021;2021(48):5077–84.

12. Ivanov, S. B., Davidovich, R. L., Mikhailov, Yu. N., Shchelokov, R. N. Koord. Khim.(Russ.)(Coord. Chem.), 1982, 8, 211.

13. Wang CM, Liao CH, Kao HM, Lii KH. Hydrothermal Synthesis and Characterization of [(UO2)2F8(H2O)2Zn2(4,4‘-bpy)2]·(4,4‘-bpy), a Mixed-Metal Uranyl Aquofluoride with a Pillared Layer Structure. Inorg Chem. 2005 Sep 1;44(18):6294–8.

14. Bombieri G, De Paoli G, Immirzi A. An example of uranium(IV) insertion within a macrocyclic crown ether with coexistence of the metal in two oxidation states. Journal of Inorganic and Nuclear Chemistry. 1978 Jan 1;40(11):1889–94.

15. Mak TCW, Wai-Hing Y. Synthesis and crystal structure of bis(tetramethylammonium) aquotetra-fluorodioxouranate(VI) dihydrate, [(CI3)4 N]2[UO2 F4(H2 O)]·2H2O. Inorganica Chimica Acta. 1985 Mar 1;109(2):131–3.

16. Zhang Y, Lu K, Liu M, Karatchevtseva I, Tao Z, Wei G. Thorium(IV) and uranium(VI) compounds of cucurbit[10]uril: from a one-dimensional nanotube to a supramolecular framework. Dalton Trans. 2020 Jan 2;49(2):404–10.

17. Hassaballa H, Steed JW, Junk PC. New insights into the formation of extended supramolecular architectures from simple building blocks. Chem Commun. 1998 Jan 1;(5):577–8.

18. Hassaballa H, Steed JW, Junk PC, Elsegood MRJ. Formation of Lanthanide and Actinide Oxonium Ion Complexes with Crown Ethers from a Liquid Clathrate Medium. Inorg Chem. 1998 Sep 1;37(18):4666–71.

19. Kerr, AT, Kumalah, SA, Holman, KT, Butcher, RJ, Cahill, CL. Uranyl Coordination Polymers Incorporating η5-Cyclopentadienyliron-Functionalized η6-Phthalate Metalloligands: Syntheses, Structures and Photophysical Properties. J. Inorg. Organomet. Polym. Mater., 2014☹24):128.

20. Mikhailov, Yu. N., Ivanov, S. B., Kuznetsov, V. G., Davidovich, R. L., Koord. Khim. (Russ.)(Coord. Chem.), 1979:(5):1545.

21. Ok KM, O'Hare D. Hydrothermal synthesis, crystal structure, and characterization of a new pseudo-two-dimensional uranyl oxyfluoride, [N(C2H5)4]2[(UO2)4(OH2)3F10]. Journal of Solid State Chemistry. 2007 Feb 1;180(2):446–52.

22. Yue Z, Lin J, Silver MA, Han L, Li X, Zhou J, et al. Anionic uranyl oxyfluorides as a bifunctional platform for highly selective ion-exchange and photocatalytic degradation of organic dyes. Dalton Trans. 2018 Oct 30;47(42):14908–16.

23. Liu XX, Wang Y, Tian WG, Yang W, Sun ZM. Heterometallic zinc uranium oxyfluorides incorporating imidazole ligands. Chinese Chemical Letters. 2015 Jun 1;26(6):641–5.